Chemosphere 313 (2023) 137518

Contents lists available at ScienceDirect

Chemosphere

journal homepage: www.elsevier.com/locate/chemosphere

Norfloxacin mineralization under light exposure using Sb–SnO_2 ceramic anodes coated with $BiFeO_3$ photocatalyst

C. Domingo-Torner [a], M. García-Gabaldón [a], M.C. Martí-Calatayud [a], S. Mestre [b], V. Pérez-Herranz [a,*]

[a] IEC Group, Universitat Politècnica de València, Camí Vera s/n, Valencia, Spain
[b] ITC, Universitat Jaume I, Av. Vicent Sos Baynat s/n, Castellón, Spain

HIGHLIGHTS

- $BiFeO_3$ coating showed an increase of the photoactivity of the Sb–SnO_2 ceramic anode.
- EIS showed a reduction of the charge transfer resistance with the $BiFeO_3$ coating.
- Norfloxacin mineralization increased with current density and light.
- MCE and energy consumption of the system were improved in presence of light.

GRAPHICAL ABSTRACT

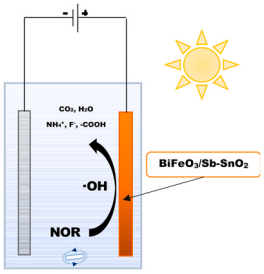

ARTICLE INFO

Keywords:
Norfloxacin
Mineralization
Photocatalyst
BiFeO3 layer
Sb–SnO2 ceramic electrode
Advanced oxidation processes

ABSTRACT

Advanced Oxidation Processes have been proven to be an efficient way to remove organic pollutants from wastewaters. In this work, a ceramic electrode of Sb–SnO_2 (BCE) with a layer of the photocatalytic material $BiFeO_3$ (BFO-BCE), has been characterized electrochemically and further tested for norfloxacin photoelectrooxidation in the presence and absence of light. The electrode photoactivity was highly enhanced thanks to the presence of $BiFeO_3$, as confirmed by Linear Sweep Voltammetry, chronoamperometry and potentiometry, and Electrochemical Impedance Spectroscopy. Additionally, working in galvanostatic mode, a high mineralization of norfloxacin was achieved after 240 min, reaching 62% at 25 mA cm^{-2} under light conditions. This value is comparatively higher than the 40% achieved with the BCE. The oxidation byproducts were followed by ionic chromatography and HPLC analysis, which also allowed us to propose an oxidation pathway of the norfloxacin molecule. Finally, some indicators of the reactor performance such as the Mineralization Current Efficiency and the specific energy consumption were analyzed, revealing that lower current densities (8.3 mA cm^{-2}) led to higher current efficiencies, and that light improved both the current efficiency and energy consumption.

1. Introduction

Emerging pollutants have been paid great attention in recent years because of their innate hazard to human health and natural ecosystems. Among them, pharmaceuticals are typically found in wastewater due to their massive consumption rates (Abbassi et al., 2016; Balu et al., 2022;

* Corresponding author. .
E-mail address: vperez@iqn.upv.es (V. Pérez-Herranz).

https://doi.org/10.1016/j.chemosphere.2022.137518
Received 6 September 2022; Received in revised form 24 November 2022; Accepted 7 December 2022
Available online 7 December 2022

Bao et al., 2021). Particularly, antibiotics have been widely used during the past decades, making them one of the most spread pollutants in water courses (Shurbaji et al., 2021). Their accumulation in natural environments may lead to toxic effects, due to their interaction with other compounds, as well as to increased antimicrobial resistance, which can imply a lower success rate on treating infections (Ashfaq et al., 2016). Norfloxacin (NOR) is one of the most used antibiotics and a member of the family of fluoroquinolones. It is a synthetic antibacterial agent used for a variety of respiratory, urinal and biliary infections, not only for human treatments, but also for veterinary purposes (Lavaee et al., 2017).

Attending to the difficulty of eliminating this kind of pollutants by the conventional methods available in Wastewater Treatment Plants (WWTPs) (Yu et al., 2020), many studies are bringing attention to Electrochemical Advanced Oxidation Processes (EAOPs) using different anode materials. In our previous work (Mora-Gomez et al., 2019), the performance of a Boron Doped Diamond (BDD) electrode was compared with that of a basic ceramic electrode made of SnO_2 doped with Sb (referred to as BCE in this work). The ceramic electrodes showed to be a promising material for the degradation of NOR with a low economical investment compared to BDD, which despite showing higher degradation and mineralization rates, is significantly more expensive. In (Mora-Gómez et al., 2020), the reactor configuration for the BDD and BCE anodes was evaluated in order to further characterize the BCE performance. There, the target compound was the β-blocker atenolol, and the BCE electrode achieved mineralization rates of up to 27.3% and 39.2% using an undivided reactor and a reactor divided by a membrane, respectively, both after 90 min at a current density of 50 mA cm^{-2}. Further investigations were carried out to improve the BCE electrode. In (Carrillo-Abad et al., 2020b), CuO was added to the BCE in the sintering process in order to enhance its electrical and electrochemical performance. However, no promising results were observed when compared to the BCE. For such reason, a further step was carried out by means of adhering photocatalytic materials to the BCE surface. In this regard, the main issue for the use of BCE as photoanode is that, even if it has some level of photoactivity, its high band gap (around 3.7 eV) reduces the light spectra that can be absorbed (Kim et al., 2018). This is why reducing its bandgap by coating the BCE with other photocatalysts has been proposed. By using this approach, the need to separate the photocatalysts from the treated effluent is also avoided (Daghrir et al., 2012; Su et al., 2016). Different materials are suitable for this purpose, mainly mixed oxides such as wolframates (Bi_2WO_6 (Zhao et al., 2007b), $ZnWO_4$ (Zhao and Zhu, 2006)) and spinels ($ZnFe_2O_4$ (Kumbhar et al., 2015), $CdFe_2O_4$ (Harish et al., 2012)), but also bismuth compounds, such as $BiPO_4$ (Zeng et al., 2015), $BiVO_4$ (Zhang et al., 2016) or Bi_2MoO_6 (Zhao et al., 2007a), have received increasing attention as photocatalytic coatings. Among bismuth compounds, $BiFeO_3$ has been selected as the material for the present investigation.

$BiFeO_3$ (BFO) is considered a multiferroic material because it presents antiferromagnetic, ferroelectric and ferroelastic properties (Wu et al., 2012). It excels as a semiconductor material because of its bandgap of around 2.2 eV (Liao et al., 2021) at room temperature as well as its high chemical stability (Gulati et al., 2022; Y. Guo et al., 2017). In addition, its photocatalytic and photoelectrical properties vary under visible-light exposure, which has motivated many research studies about its applications in the field of electrochemistry. BFO is a material that in its bulk state presents very weak ferromagnetic properties at room temperature, as well as a high current leakage caused by structural defects. However, thin films of this material showed an enormous improvement in its polarization and ferroelectric properties in comparison to its bulk version (Catalan and Scott, 2009; Pradhan et al., 2005).

Many examples confirm these improved properties of BFO thin films, in (Farhadi et al., 2021) BFO synthesized on reduced graphene oxide showed up to 90% of oxidation of acetimophen, and even more (98.6%) when doped with other metals such as La. Another example is (Nkwachukwu et al., 2021), where photoanodes made of La–BFO deposited over a fluorine-doped tin oxide substrate were tested for the elimination of different organic dyes (congo red, methanol blue or orange II), showing elimination rates up to 84.2% within 2 h. Their applications in pharmaceuticals oxidation were also demonstrated in (Sharmin and Basith, 2022), where gadolinium doped $BiFeO_3$ nanoparticles degraded up to 80% of ciprofloxacin and 79% of levofloxacin under solar light.

Many different ways of creating $BiFeO_3$ thin films have been proposed in the literature such as sol-gel processing (Deepak Sharma and Basantakumar Sharma, 2022), chemical solution deposition (CSD) (Wang et al., 2022), or dip coating (Alam et al., 2018). Dip coating has been highlighted as one of the most reliable procedures along with sol-gel to produce $BiFeO_3$ thin films. This technique consists of using a suspension of small particles and fixing them by a thermal treatment. The main advantage is the simplicity and cost efficiency when compared to other advanced techniques (Gumiel and Calatayud, 2021).

In the present work, taking into consideration the properties and capabilities of the BFO to act as a photoelectric enhancer, a photoanode consisting of a BCE electrode coated via dip coating with a BFO layer is characterized and tested for the mineralization of norfloxacin in the presence and absence of a source of light.

2. Material and methods

2.1. Materials and chemicals

SnO_2 (purity 99.85%, Quimialmel S.A., Spain), Sb_2O_3 as dopant (purity 99%, Alfa-Aesar, Germany) and polyvinylalcohol (PVA, Mowiol 8–88, Clariant Iberica S.A. Spain) were purchased for the BCE electrode synthesis. Additionally, iron oxide (Panreac Química S.A.U. Spain), bismuth oxide (Quimialmel S.A., Spain) and isopropyl myristate (Quimidroga S.A. Spain) were used for the $BiFeO_3$ synthesis.

For the photo-electrooxidation experiments, a commercial norfloxacin pill of 400 mg from Cinfa was purchased from a drugstore, whereas for the elaboration of reference standards, analytical standard norfloxacin (>98%) was purchased from Sigma-Aldrich, analytical grade anhydrous sodium sulfate (99%) from Sigma-Aldrich and sulfuric acid (95–97%) was obtained from J.T Baker. Distilled water was used to prepare the norfloxacin solutions.

Sodium hydrogen carbonate (>99%), anhydrous sodium carbonate (>99%) and nitric acid/dipicolinic acid used to perform the ionic chromatography measurements were purchased from Sigma-Aldrich.

Sodium thiosulfate from Sigma-Aldrich, potassium iodide (>99%) from Honeywell and a starch solution of 1% from PanReac Applichem were used to analyze the persulfate content.

Acetonitrile hypergrade for LC-MS from Merck, acetic acid optima for LC-MS from Fischer Chemical and ultrapure type 1 water were used to prepare the dilutions for the HPLC analysis.

2.2. Electrode synthesis

The substrate material for the electrode was manufactured using SnO_2 and Sb_2O_3 as dopant in a mole ratio 99/1. The ligand was polyvinylalcohol, which was added in a 0.8 wt%. The processing conditions employed for the electrode's synthesis were described elsewhere (Carrillo-Abad et al., 2020b). Flat specimens of 80x20 × 5 mm were obtained by dry pressing the wet powder in a laboratory automatic press SS-EA (Nannetti Srl, Italy), working at 250 kg cm^{-2}. The electrodes were sintered in a laboratory furnace (RHF1600, Carbolite Furnaces Ltd, UK). The temperature profile consisted of heating at 5 °C min^{-1} from room temperature to 1200 °C, keeping 1 h at maximum temperature and subsequent cooling.

The precursors of the $BiFeO_3$ were iron oxide and bismuth oxide. The raw materials were mixed in a mortar using ethanol as solvent. The dry mixture was calcined in an electric furnace (RHF1600, Carbolite

Furnaces Ltd., UK) using a mullite crucible with a porcelain lid. The thermal treatment was heating at 10 °C min^{-1} up to 800 °C, a soaking time of 4 h and cooling. The product was grinded in an agate mortar and the powder was characterized and used to obtain the suspension for dip coating. The suspension was prepared milling a mixture of powder and isopropyl myristate in a planetary mill with microballs (Pulverisette 5, Fritsch GmbH, Germany) for 60 min at 260 rpm. The suspension has a 0.6 wt% in $BiFeO_3$ as previous experiments showed that this ratio produced a better-quality layer on the electrode. The deposition of the catalyst by dip coating was carried out in a homemade apparatus, which enables the control of immersion and emersion speeds. After the deposition, the electrodes were dried in an oven and the catalyst was thermally fixed with a treatment, based on heating at 10 °C min^{-1} up to 800 °C and 1 h of soaking time, in an electric furnace (RHF 1400, Carbolite Furnaces Ltd. UK).

2.3. Structural characterization of the electrodes

The bulk density of the sintered electrodes was measured by mercury immersion (Archimedes' method). The electrical resistivity of the sintered samples was measured by a four points method with a HIOKI RM3545 equipment (Hioki E.E. Corporation, Japan).

Characterization of crystalline structures was performed using an X-ray diffractometer (Theta-Theta D8 Advance, Bruker, Germany), with CuK radiation ($\lambda = 1.54183$ Å). The generator applied a light intensity of 45 kV and 40 mA. XRD data were collected by means of a VÅNTEC-1 detector in a 2θ from 5 to 90° with a step width of 0.015° and a counting time of 1.2 s/step. Images of the electrode's surface metalized with Pt were taken from FEG-SEM (QUANTA 200 F, FEI Co, USA) with microanalysis to identify the characteristics and the composition of the catalyst's particles.

2.4. Electrochemical characterization of the electrodes

A prismatic reactor made of quartz and filled with 200 mL of 0.1 M sodium sulfate was used. The electrochemical characterization was conducted using a three-electrode configuration, where an Ag/AgCl electrode (Metrohm) was employed as a reference electrode. The counter electrode was a Pt foil of 1 cm^2 (Mettler Toledo) and the working electrodes were the BCE and BFO-BCE with a working area of 0.25 cm^2.

Linear sweep voltammetries (LSV) were carried out using an Autolab PGSTAT302N Potentiostat/Galvanostat (Metrohm), with a scan rate of 50 mV s^{-1}, starting from the open circuit potential (OCP) until reaching 2 V over the OCP in the positive direction. LSV experiments were conducted with and without light using a Hamamatsu Lightningcure LC8 device with a 200 W Xenon lamp. A light filter A9616-08 was installed in order to block the infrared light, only allowing the visible light spectra. All experiments were done at room temperature. Light pulsed chronoamperometry at 0.5 V over the OCP was performed using the same configuration, applying pulses of light and pauses of 150 s each. Light pulsed chronopotentiometric experiments were also performed until the stationary state was reached at an applied current density of 5.2 mA cm^{-2}, this value was selected from the previous chronoamperometric measurements.

Electrochemical Impedance Spectroscopy (EIS) was performed using the same set-up beforementioned, where a DC potential value of 0.5 V over the OCP in the presence and absence of light was tested. A frequency range between 100 kHz and 10 mHz and an AC signal amplitude of 5 mV were used.

2.5. Photo-electrooxidation experiments

The norfloxacin photo-electrooxidation experiments were carried out in the 200 mL prismatic quartz reactor beforementioned with a solution of 100 mg L^{-1} of norfloxacin and 2 g L^{-1} of sodium sulfate as a supporting electrolyte. The experiments were conducted under stirring conditions and at room temperature. The working electrode was the BFO-BCE with an effective area of 24 cm^2 and the cathode was an AISI 304 stainless steel sheet of the same surface area. The reference electrode was the Ag/AgCl mentioned before.

The experiments lasted 4 h each and were carried out under two different galvanostatic conditions: 25 and 8.3 mA cm^{-2} using a Peaktech P 1585 laboratory power supply. All the experiments were tested with and without light, by using the light source beforementioned. A 2 mL sample was taken every 15 min during the first hour; afterwards, the samples were collected every 30 min.

2.6. Analytical methods

The NOR mineralization was determined by measuring the total organic carbon (TOC) in a Shimadzu TNM-L ROHS TOC analyzer and the identification of the different ionic species was carried out by a Metrohm 883 Basic IC Plus Ionic Chromatograph. Additionally, the persulfate content was analyzed by iodometric titration (Mora-Gómez et al., 2020).

Ultra-High Performance Liquid Chromatography and Mass Spectrometry (UHPLC-Q-TOF/MS) was used for identifying the intermediate compounds formed during the degradation, as well as to qualitatively corroborate the evolution of NOR concentration. The device was an Agilent 1290 Infinity UHPLC with a ZORBAX Eclipse Plus C18 column. The sample injection volume was 10 μL and the column temperature was 30 °C. The analysis was performed using ultrapure type 1 water with 0.1% acetic acid as eluent A and acetonitrile as eluent B, in a gradient elution mode of 0.2 mL min^{-1} flow rate. This elution gradient began with 10% of B and then increased up to 30% of B in 7 min, then decreased to 0% B in 13 min, after that it stayed stationary in 0% B for 1 min, then increased again to 10% of B in 2 min and finally stayed stationary in 10% of B for 7 min. A mass spectrometer attached to the HPLC system worked with a positive electrospray ionization, a 4 kV capillary voltage, a 30 psi pressure nebulizer and a drying gas flowrate of 11 L min^{-1} at 350 °C.

2.7. Indicators of the reactor performance

In order to assess the performance of the electrodes referred to the mineralization of NOR, the mineralization current efficiency (MCE) and the energy consumption were analyzed. The MCE was calculated, using Eq. (1) (Xu et al., 2022; Zhang et al., 2022).

$$MCE = \frac{n\ F\ V\ \Delta TOC_t}{7.2\ 10^5\ m\ I\ t} 100\% \quad (1)$$

where n is the number of electrons exchanged in the system assuming a complete mineralization towards CO_2 according to the oxidation of NOR shown in Eq. (2), F is the Faraday constant (C mol^{-1}), V is the reactor volume in L, ΔTOC_t is the difference in TOC values between the sampling time t and the initial value (mg L^{-1}), $7.2{\cdot}10^5$ is a unit correction factor, m is the number of carbon atoms in the NOR molecule and I is the applied current.

$$C_{16}H_{18}FN_3O_3 + 29H_2O \rightarrow 16CO_2 + 3NH_4^+ + F^- + 64H^+ + 66e^- \quad (2)$$

The energy consumption per unit of TOC removal in kWh $kgTOC^{-1}$ was calculated following Eq. (3).

$$E = \frac{\int_0^t U(t)\ I(t)\ dt}{\Delta TOC_t\ V} \quad (3)$$

Where $U(t)$ is the experimental cell voltage in V.

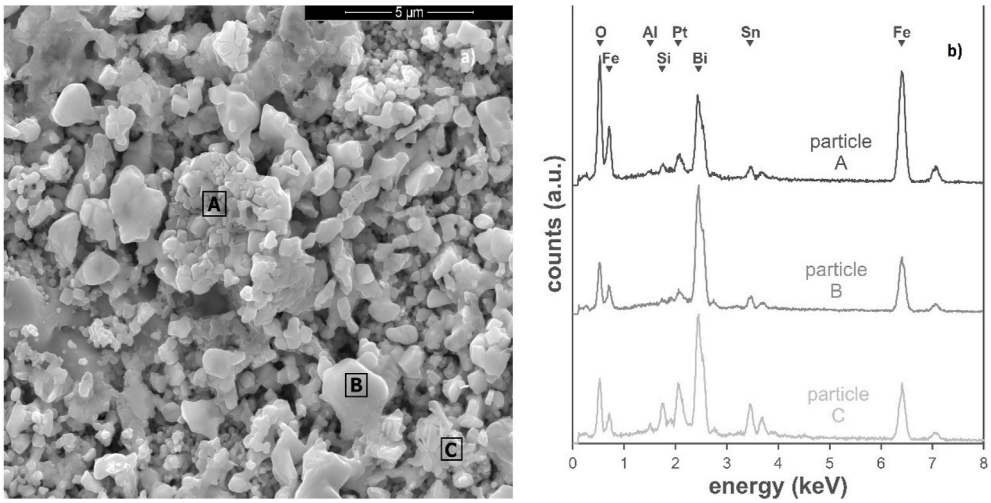

Fig. 1. SEM image of electrode's surface (a) and EDX analysis (b) of the particles A, B and C.

3. Results and discussion

3.1. Electrode characterization

A surface analysis was performed in order to evaluate the dip coating procedure over the BCE. The ceramic electrodes showed a grey-bluish color, characteristic of the solid solution of antimony oxide in tin oxide. Their porosity was estimated to be around 50%, taking into account the bulk density of the electrodes (3401 ± 14 kg m^{-3}) and the true density of tin oxide. The mean resistivity of the specimens was 0.0228 ± 0.0005 Ω cm, which is low enough to act as a ceramic electrode.

The solid-state reaction generated a reddish product, which was difficult to grind. The diffractogram (Fig. S1) showed that the reaction was uncompleted as the product included two compounds of Bi and Fe ($BiFeO_3$ and $Bi_2Fe_4O_9$), jointly with an unexpected mixed oxide of bismuth and silicon, which was probably the result of the interaction of the reacting mixture with the mullite crucible. This result agrees with the work of Liu et al., which describes the difficulties to obtain pure $BiFeO_3$ and the limited stability interval (Liu et al., 2011).

The microstructure of the electrode's surface after the catalyst deposition showed three kinds of particles with different composition (Fig. 1a and b). Agglomerates of particles with cubic-like morphology rich in Fe, Bi and O which could correspond to $Bi_2Fe_4O_9$ phase (signaled with A). Rounded particles rich in Bi and with lower proportion of Fe and O could correspond to $BiFeO_3$ (signaled with B). Finally, agglomerates of lamellar-like particles which contain Si in addition to Bi, O and Fe could correspond to $Bi_{24}Si_2O_{40}$ generated by reaction with the crucible (signaled with C).

The LSV obtained with the BFO-BCE and the BCE anode in presence and absence of external light are shown in Fig. 2a. In this figure, the X axis represents the overpotential applied over the OCP during the LSV. As expected, the BFO-BCE shows a higher current density value than the BCE for the entire range of scanned potentials, indicating that the resistance to charge transfer decreased thanks to the $BiFeO_3$ coating. It is remarkable that the electrode requires the application of an external potential in order to register the photocurrent values. Also, it can be noticed that depending on the applied potential, the effect of light on the registered photocurrent varies: it is higher at intermediate values of the overpotential range. In Fig. 2b the photocurrent evolution with the overpotential is represented. Here the maximum difference between the experiments in presence and absence of light is achieved at around 0.75 V over the OCP, with a photocurrent value around 0.94 mA cm^{-2}. This characteristic evolution with a maximum, has been previously seen in the work of (Malviya et al., 2017), and it is thought to be caused by the microstructure of the electrode. Towards the end of the potential scan rate, the gas generation is greater due to the higher potentials applied, and the pores of the structure are gradually filled with it. The gas accumulation within the porous structure of the electrode, which is hard to remove, increases the resistance of the system and reduces the current flow through the electrode and, therefore, also the effect of light on the current density.

Fig. 2c shows the chronoamperometric curves obtained with the coated BFO-BCE electrode working at a potential of 0.5 V over the OCP, where light pulses were performed to confirm the photoactivity of the electrode after the addition of the $BiFeO_3$ to the Sb–SnO_2 porous structure. An immediate change in the current density values can be noticed when light is applied, however a 60–70 s window is required to achieve a steady-state value. Also, a period of 150 s seemed to be necessary to achieve the relaxation of the electrode response after switching off the light. This test showed an average increase of around 3.1 mA cm^{-2} in the photocurrent response. This corroborates a clear effect of the $BiFeO_3$ coating in the photoactivity performance of the electrode. This enhancement is related to the fact that after the incidence of UV–visible light in the $BiFeO_3$ coating, the electrons are excited from the valence band up to the conduction band, leaving behind holes in the valence band. This generation of charge carriers is well studied in literature (Gulati et al., 2022; Soltani and Lee, 2020), and is the responsible for the current increase under light conditions.

The photocatalytic activity of $BiFeO_3$ in terms of photocurrent at a given electrode potential has been demonstrated in Fig. 2c. However, in real applications it is common to operate at constant current density (galvanostatically) or at constant cell voltage. Operating an electrochemical reactor galvanostatically involves setting the rate of the electrochemical reactions, i.e., in the case of an electrochemical advanced oxidation process, setting the rate of ·OH generation. Therefore, in this mode of operation, the photocatalytic activity of $BiFeO_3$ can be expected to result in a change in the electrode potential. To confirm this, a chronopotentiometry study under light pulses was also performed and the results are presented in Fig. 2d. The applied current density value (5.2 mA cm^{-2}) was selected based on the chronoamperometry performed previously, which registered this average value, as seen in Fig. 2c. Here the action of light on the electrode reduces the electrode potential, and it was applied until a steady-state value was achieved. Later comes a relaxation period, where the potential increases again until the original value is attained again. This evolution is the same for every light pulse, which indicates a reversibility in the effect of the light, i.e., the potential values decreased under the application of light thanks to the BFO layer, which reduces the charge transfer resistance.

EIS analyses were also performed to gather qualitative information about the electrochemical behavior of the system. The spectra obtained

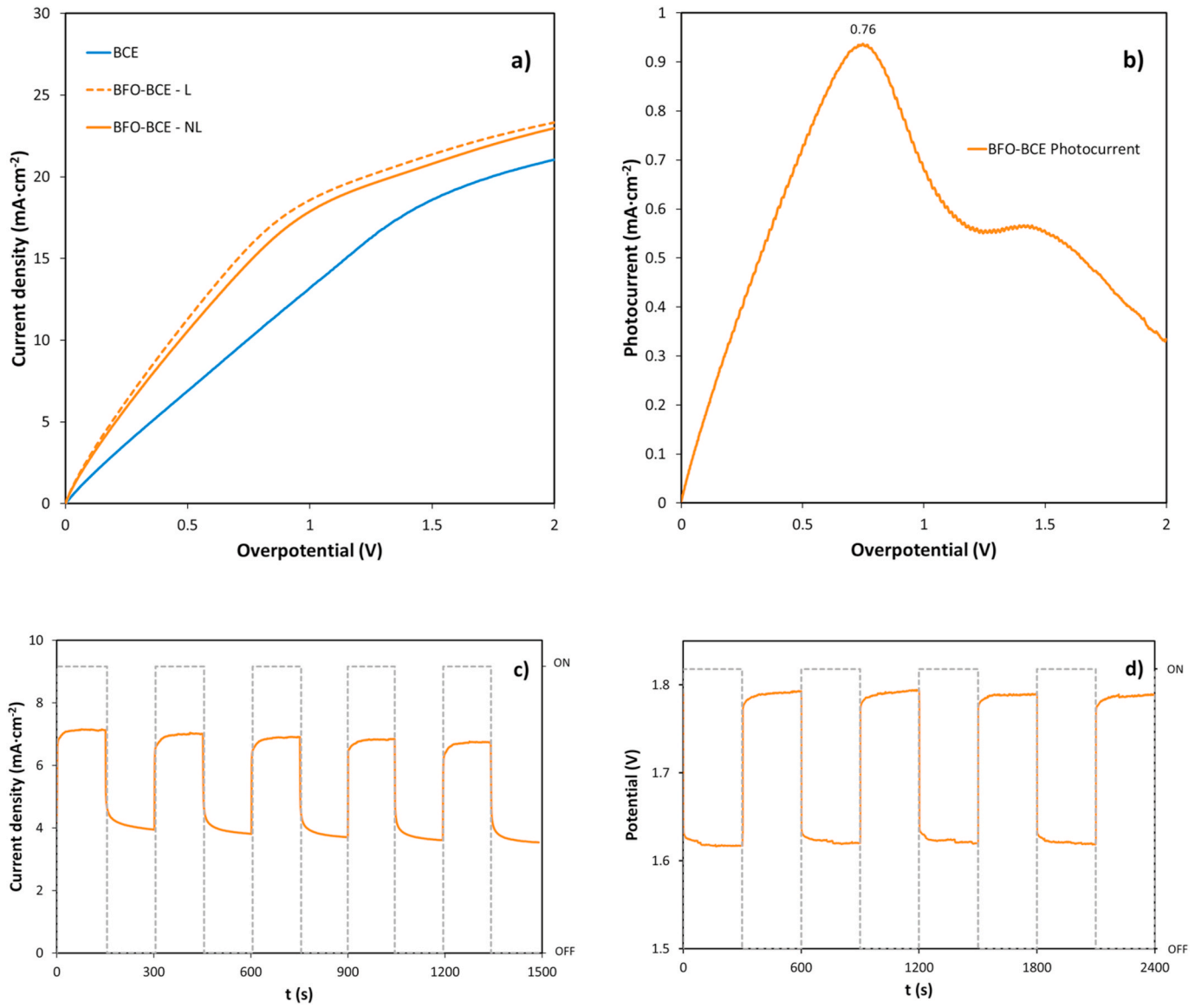

Fig. 2. (a) LSV of the BFO-BCE and BCE anodes in a 0.1 M Na_2SO_4 solution in presence (L) and absence (NL) of light (b) BFO-BCE photocurrent evolution under light effect. (c) Chronoamperometry using light pulses for the BFO-BCE electrodes, applying an overpotential of 0.5 V. (d) Chronopotentiometry using light pulses for the BFO-BCE electrode, applying 5.2 mA cm^{-2}.

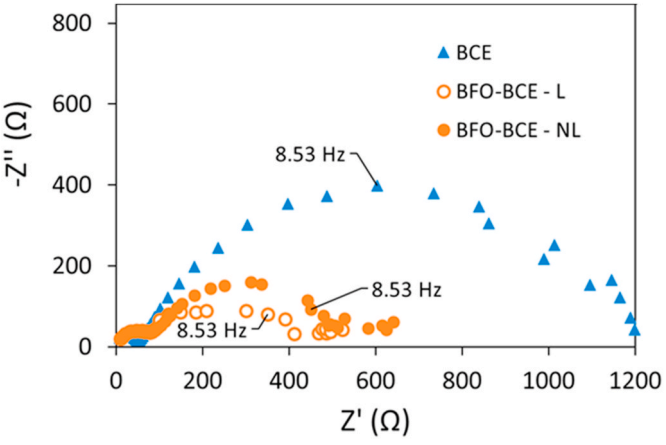

Fig. 3. EIS analyses for 0.5 V over the OCP in presence (L) and absence of light (NL), for the BCE and the BFO-BCE.

for the different experiments are presented in Fig. 3. Nyquist plots obtained at a DC voltage signal of 0.5 V over the OCP are represented for the BCE and the BCE-BFO. It is observed a clear effect of the $BiFeO_3$ coating, where a lower resistance related to the radius of the second semicircle, associated with the charge transfer resistance, is obtained in comparison to the BCE electrode. This indicates that the $BiFeO_3$ enhances the current flow of the basic electrode. When light is applied, it is observed that the resistance associated with the charge transfer resistance also decreases (Liu et al., 2000; Wang et al., 2016)). For the BCE, a resistance of 1198 Ω was obtained, whereas for the BFO-BCE in absence of light was around 495 Ω and 411 Ω in presence of it. This indicates that the BFO-BCE electrode presents an ease to transfer photogenerated electron-hole groups. Also, the maximum of the semicircle for the BCE, achieved at 8.53 Hz, is displaced to the right end of the semicircle with the addition of $BiFeO_3$ and even further in the presence of light, indicating an acceleration of the electrochemical process, since this maximum in the $BiFeO_3$ experiences is achieved at higher frequencies.

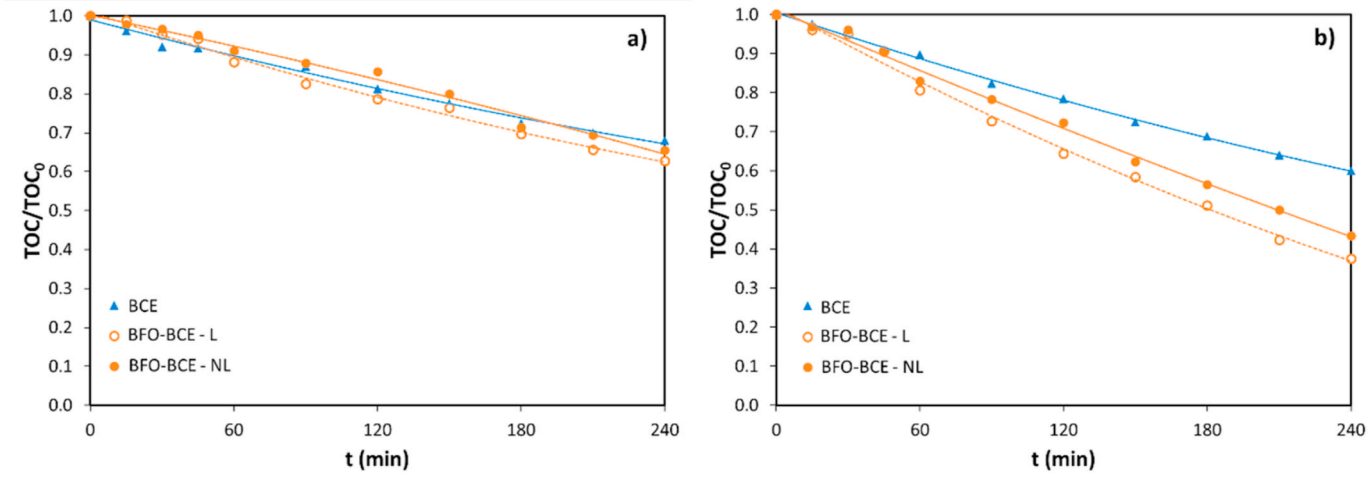

Fig. 4. TOC/TOC_0 evolution profile for current densities of a) 8.3 mA cm^{-2} and b) 25 mA cm^{-2} in presence (L) and absence of light (NL).

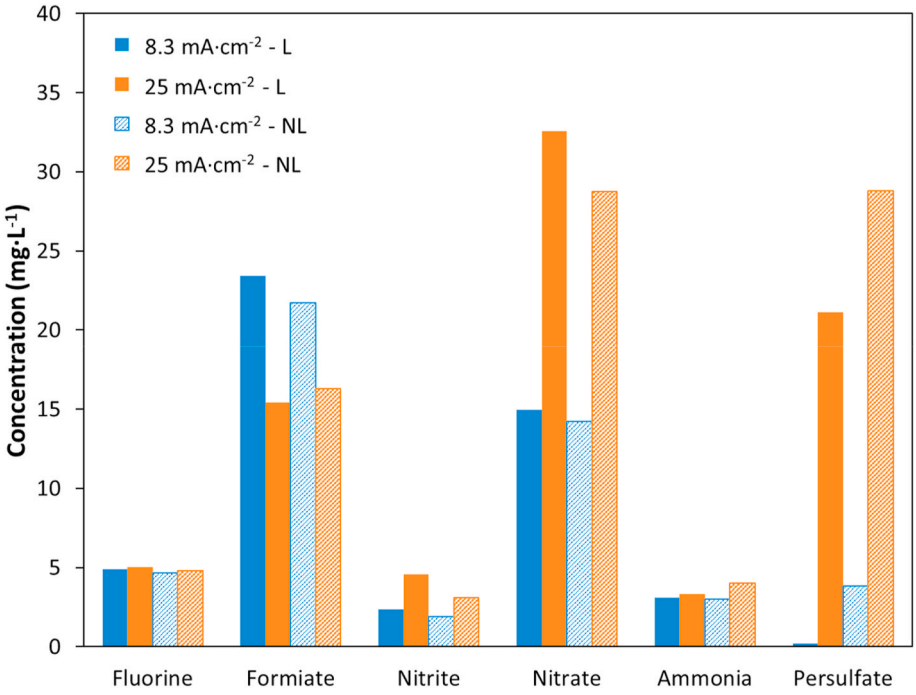

Fig. 5. Ionic composition of every experience after 4h in presence (L) and absence (NL) of light.

3.2. Photo-electrooxidation experiments

The mineralization of NOR is observed in Fig. 4, where the evolution of TOC/TOC_0 is shown for the different experiments. Light enhances mineralization in every situation, although at lower current density values mineralization rates are more similar (Fig. 4a). The highest mineralization is achieved at 25 mA cm^{-2} in presence of light, with a 62% of NOR being mineralized (Fig. 4b), whereas at 8.3 mA cm^{-2} only 37% was achieved (Fig. 4a). In absence of light, mineralization rates around 56% and 34% for 25 mA cm^{-2} and 8.3 mA cm^{-2} were achieved, respectively. This indicates a 6% increase for 25 mA cm^{-2} and 3% for 8.3 mA cm^{-2}. For the BCE, around 40% of NOR was mineralized at 25 mA cm^{-2}; this value being higher than the 32% obtained at 8.3 mA cm^{-2}. Higher mineralization rates in presence of light are related to the fact that $BiFeO_3$, under light exposure, increases the formation of ·OH radicals that react with the NOR molecule and its intermediates, oxidizing it to CO_2 and other inorganic byproducts. The formation of ·OH in photocatalysts (He et al., 2013) is achieved by the effect of light over the material, which excites the electrons (e^-_{CB}), promoting them to the conduction band and leaving behind their associated holes (h^+_{VB}) in the valence band (Eq. (4)). These holes, in need of electrons, react either with the NOR molecule directly, degrading it, or with the H_2O present in the media, producing ·OH which also degrade the NOR molecules (Eq. (5)). Also, the electrons can react with dissolved O_2, an electron scavenger, reducing it to $O_2^{\cdot-}$ (Eq. (6)) that also transforms into ·OH radicals through further reactions (Eq. (7), Eq. (8) and Eq. (9)) (Huang and Scott, 2018; Wang and Xu, 2012).

$$BFO - BCE + UV - energy \rightarrow e^-_{CB} + h^+_{VB} \quad (4)$$

$$h^+_{VB} + H_2O \rightarrow H^+ + {}^{\cdot}OH \quad (5)$$

$$e^-_{CB} + O_2 \rightarrow O_2^{\cdot-} \quad (6)$$

$$O_2^{\cdot-} + e^-_{CB} + 2H^+ \rightarrow H_2O_2 \quad (7)$$

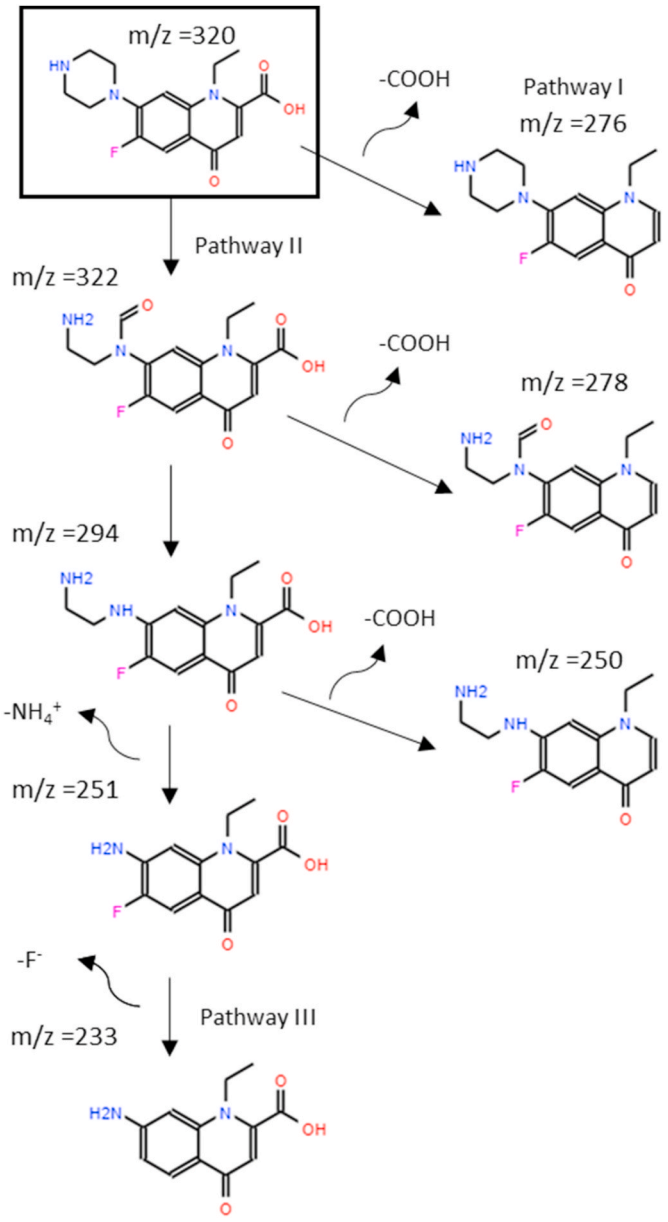

Fig. 6. Proposed degradation route for NOR molecule via HPLC analysis.

$$H_2O_2 + e^-_{CB} \rightarrow {}^{\cdot}OH + OH^- \quad (8)$$

$$H_2O_2 + O_2^{\cdot-} \rightarrow {}^{\cdot}OH + OH^- + O_2 \quad (9)$$

For a further evaluation of the mineralization process of the NOR molecule, an analysis of ionic by-products was performed. The ions detected in the ion chromatography were short-chain organic molecules such as formiate and low traces of acetate as well as other inorganic ionic species derived from the original molecule such as fluorine, nitrate, nitrite and ammonia. As seen in Fig. 5, the presence of fluorine is an indicative of the proper rupture of the NOR molecule and the release of the F atoms present in it in the form of F^- ions. The process of this degradation step of NOR is very similar in all cases showing insignificant variations due to the effect of current density or light. The detection of formiate proves the generation of organic intermediates during the degradation of NOR. It is remarkable that, at lower values of current density, the concentration of formiate detected is higher. This happens because although lower current densities eliminate a lower amount of NOR molecules producing short-chain carbon molecules (i.e., formiate), the rate of generation of these organic intermediates is higher than the rate at which they are fully oxidized to CO_2; therefore, their concentration keeps increasing with time. Regarding the evolution of nitrite, nitrate and ammonia, a higher oxidation degree of the nitrogen present in NOR was achieved at high current values and, therefore, it is deduced that a higher concentration of oxidating species is present in these experiences. Theoretically, the nitrogen present in the NOR molecule tends to form NH_4^+ as depicted earlier in Eq. (2), however as time passes, ammonia ions are further oxidized to nitrite and later to nitrate as observed in Fig. 5.

The results obtained for the persulfates are also depicted in Fig. 5, where a clear effect of light is observed. Light reduces the number of persulfates at both current density values, being even undetected at 8.3 mA cm^{-2} under light exposure. At 25 mA cm^{-2} in presence of light, there is around a 27% less persulfates than in absence of it, and for 8.3 mA cm^{-2} a 100% less. As it was observed in a previous work (Montañés et al., 2020) the oxidation process of NOR in presence of Na_2SO_4 as a supporting electrolyte can lead to the formation of persulfates ($S_2O_8^{2-}$) after the oxidation of SO_4^{-2} ions. Persulfate ions increase the toxicity of the effluent, therefore here it can be concluded that light reduces the toxicity of the oxidation process. This decrease of persulfate concentration is related to their activation under light exposure. When exposed to light, semiconductors generate electron-hole pairs that can react to generate hydroxyl radicals, as previously stated, but also with $S_2O_8^{-2}$ to generate $SO_4{}^{\cdot-}$ and also ·OH (Tian et al., 2022). This is supported by the results in the mineralization process of NOR (Fig. 4a and b), where under light conditions the mineralization is higher; and also, in other works

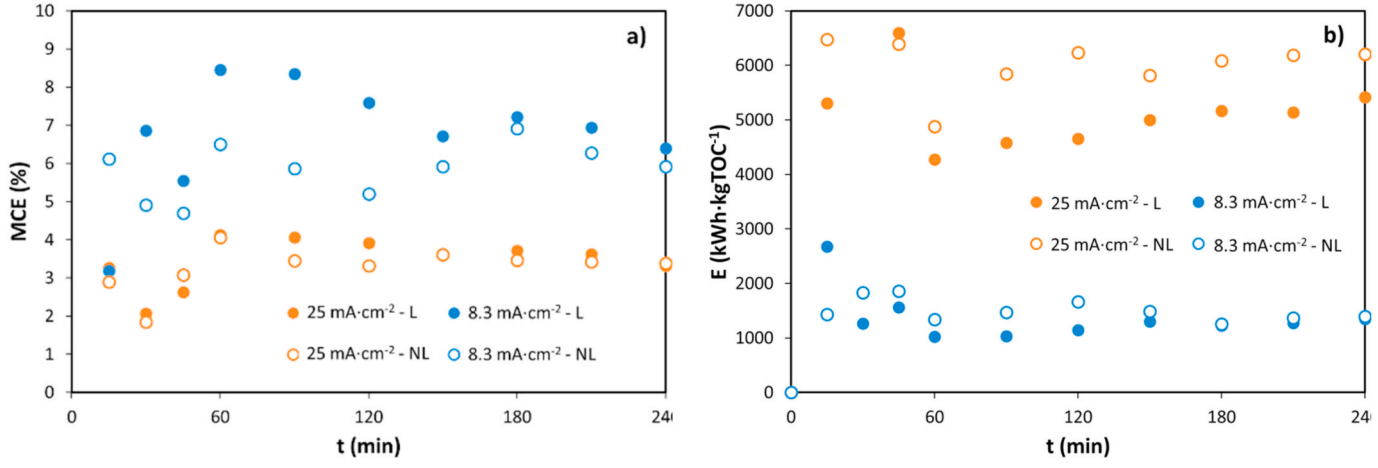

Fig. 7. MCE (a) and energy consumption (b) for 8.3 mA cm^{-2} and 25 mA cm^{-2} in prese'nce (L) and absence (NL) of light.

(Gong et al., 2018), where the addition of persulfates greatly enhanced the degradation of an organic pollutant.

Thanks to an HPLC analysis a degradation route of the NOR molecules was proposed. Not only the characteristic peak of the initial NOR molecule at $m/z = 320$ for a time value of 8.14 min was detected (Fig. S2), but also different intermediate compounds. For 8.3 mA cm^{-2}, more intermediates were detected in comparison to 25 mA cm^{-2}. In Fig. 6, a mechanism for the formation of the most relevant intermediates is proposed. The main degradation pathways involved a decarboxylation (pathway I), an opening of the piperazine ring (pathway II) and an eventual defluorination (pathway III), as also confirmed in different works (; Ma et al., 2021; Zhu et al., 2020). Initially the NOR molecule may suffer a decarboxylation leading to intermediates with $m/z = 276$. Alternatively, the NOR molecule may suffer a gradual rupture of the piperazine ring due to the ·OH radicals and further oxidation of the hydroxyl groups, leading to the intermediate of $m/z = 322$. Two options are opened afterwards, one related to a decarboxylation leading to $m/z = 278$, or a further destruction of the piperazine ring leading to $m/z = 294$. The intermediates coming after can follow two routes as detected experimentally, one with decarboxylation (having a $m/z = 250$) and the other one with a complete scission of the piperazine ring, leaving an amide behind ($m/z = 251$). Following this last route, a defluorination of the intermediate results in $m/z = 233$.

3.3. Analysis of the energy consumption

A further analysis about the mineralization current efficiency (MCE) and the energy consumption was carried out. As shown in Fig. 7, there are no clear variations with time either for the MCE or the energy consumption. MCE average values for 25 mA cm^{-2} are 3.43% and 3.25% in presence and absence of light, respectively; and 6.72% and 5.83% for 8.3 mA cm^{-2} also in presence and absence of light. The average energy consumption values are 5102 and 5927 kWh $kgTOC^{-1}$ for 25 mA cm^{-2} in presence and absence of light, respectively; and 1244 and 1521 kWh $kgTOC^{-1}$ for 8.3 mA cm^{-2} in presence and absence of light. The effect of light is clear since it increases the current efficiency and decreases the energy consumption. This effect of light was previously seen in the chronopotentiometry (Fig. 2c), where the light pulses reduced the electrode potential, which translates into a reduction of the cell potential and therefore in a lower energy consumption.

The MCE (Fig. 7a) increased under light conditions around an extra 15% at 8.3 mA cm^{-2} and 5% at 25 mA cm^{-2} in comparison with the experience in absence of light. This is achieved thanks to the formation of more ·OH radicals under light exposure as stated before. Additionally, at higher current density values the MCE is lower in both scenarios, with and without light, due to the increased relevance of parasitic reactions. These reactions are related to the high reactivity of ·OH, since a higher current density generates more ·OH capable of reacting in termination reactions instead of degrading NOR and its intermediate by-products, which reduces the current efficiency. Energy consumption rates (Fig. 7b) decrease in presence of light up to 8% in 8.3 mA cm^{-2} and around 15% in 25 mA cm^{-2}. This means that, in practice, the positive impact of light in the system is noticeable. These results are of the same order of magnitude as those obtained in previous works (Carrillo-Abad et al., 2020a, 2022; Mora-Gómez et al., 2022), where the MCE and energy consumption values were relatively similar and with small variations with time.

4. Conclusions

This work was focused on the study of a basic electrode of Sb–SnO_2, BCE, coated with a layer of $BiFeO_3$, BFO-BCE, working under galvanostatic conditions and using Na_2SO_4 as a supporting electrolyte. The purpose was to evaluate the performance of the photoanodes in the mineralization of norfloxacin in presence and absence of light and to compare it with the results obtained using the basic electrode of Sb–SnO_2.

LSV experiments showed a clear improvement of the BFO-BCE anode thanks to the addition of a $BiFeO_3$ layer, achieving higher current density values when the same potential was applied. Additionally, the light enhanced this phenomenon by increasing even more the current density obtained for a given overpotential. This was corroborated with a chronoamperometric and a chronopotentiometric study, where the photoactivity of the BFO-BCE was tested through application of light pulses. A clear increase of the photocurrent and a decrease of the potential was observed under light exposure in each case. EIS analyses also confirmed that the $BiFeO_3$ layer reduced the charge transfer resistance of the electrode, backing up the enhancement of the photocatalyst to the basic electrode.

From the photo-electrooxidation experiments, the effects of the $BiFeO_3$ coating, current density and light on the mineralization rates were also investigated. A clear improvement in mineralization rates was noticed when using the electrodes coated with $BiFeO_3$. Mineralization was greater at higher current densities (25 mA cm^{-2}), and light further enhanced this increase. In absence of light, about 56% mineralization was achieved for the BFO-BCE, meaning that light improves the results for about a 6% in this case.

The mineralization of NOR was also monitored by means of ion chromatography and HPLC analysis. The presence of short-string molecules like formiates indicated a proper destruction of the NOR molecule. Also, nitrogen-related ions like nitrate, nitrite and ammonia were detected, indicating the oxidation of the original molecule. The supporting electrolyte was also oxidized to some extent, generating persulfate ions, which contribute to increase the toxicity of the treated effluents. In this case, light reduced the number of persulfates generated during the process.

A lower current density showed better values of the MCE, up to an average of 6.72% for 8.3 mA cm^{-2} in presence of light. Energy consumption was, as expected, lower at 8.3 mA cm^{-2}, but the effect of light was more important at 25 mA cm^{-2}, where a 15% less energy was consumed in comparison to the same experiments in absence of light.

Author contribution statement

C. Domingo-Torner: Methodology, Investigation. **M. García-Gabaldón**: Conceptualization, Investigation, Writing – review & editing. **M.C. Martí-Calatayud**: Conceptualization, Validation, Investigation, Formal analysis, Writing – review & editing. **S. Mestre**: Conceptualization, Investigation, Writing – review & editing, Supervision. **V. Pérez-Herranz**: Conceptualization, Resources, Writing – review & editing, Supervision, Project administration, Funding acquisition

Declaration of competing interest

The authors declare that they have no known competing financial interests or personal relationships that could have appeared to influence the work reported in this paper.

Data availability

Data will be made available on request.

Acknowledgements

The authors thank the financial support through the project RTI2018-101341-B-C21 funded by MCIN/AEI/10.13039/501100011033/(Spain) and by FEDER A way of making Europe and AICO/2021/128 funded by Generalitat Valenciana.

Appendix A. Supplementary data

Supplementary data to this article can be found online at https://doi.

org/10.1016/j.chemosphere.2022.137518.

References

Abbassi, B.E., Saleem, M.A., Zytner, R.G., Gharabaghi, B., Rudra, R., 2016. Antibiotics in wastewater: their degradation and effect on wastewater treatment efficiency. J. Food Agric. Environ. 14, 95–99.

Alam, M., Talukdar, S., Mandal, K., 2018. Multiferroic properties of bilayered $BiFeO_3$/$CoFe_2O_4$ nano-hollowspheres. Mater. Lett. 210, 80–83. https://doi.org/10.1016/j.matlet.2017.08.097.

Ashfaq, M., Khan, K.N., Rasool, S., Mustafa, G., Saif-Ur-Rehman, M., Nazar, M.F., Sun, Q., Yu, C.P., 2016. Occurrence and ecological risk assessment of fluoroquinolone antibiotics in hospital waste of Lahore, Pakistan. Environ. Toxicol. Pharmacol. 42, 16–22. https://doi.org/10.1016/j.etap.2015.12.015.

Balu, S., Chuaicham, C., Balakumar, V., Rajendran, S., Sasaki, K., Sekar, K., Maruthapillai, A., 2022. Recent development on core-shell photo(electro)catalysts for elimination of organic compounds from pharmaceutical wastewater. Chemosphere 298, 134311. https://doi.org/10.1016/j.chemosphere.2022.134311.

Bao, C., Zhao, J., Sun, Y., Zhao, X., Zhang, X., Zhu, Y., She, X., Yang, D., Xing, B., 2021. Enhanced degradation of norfloxacin by Ce-mediated Fe-MIL-101: catalytic mechanism, degradation pathways, and potential applications in wastewater treatment. Environ. Sci. Nano 8, 2347–2359. https://doi.org/10.1039/d1en00250c.

Carrillo-Abad, J., Mora-Gómez, J., García-Gabaldón, M., Mestre, S., Pérez-Herranz, V., 2020a. Comparison between an electrochemical reactor with and without membrane for the nor oxidation using novel ceramic electrodes. J. Environ. Manag. 268 https://doi.org/10.1016/j.jenvman.2020.110710.

Carrillo-Abad, J., Mora-Gómez, J., García-Gabaldón, M., Montañés, M.T., Mestre, S., Pérez-Herranz, V., 2022. Enhanced Atenolol oxidation by ferrites photoanodes grown on ceramic SnO_2-Sb_2O_3 anodes. J. Alloys Compd. 908, 164629 https://doi.org/10.1016/j.jallcom.2022.164629.

Carrillo-Abad, J., Mora-Gómez, J., García-Gabaldón, M., Ortega, E., Mestre, S., Pérez-Herranz, V., 2020b. Effect of the CuO addition on a Sb-doped SnO_2 ceramic electrode applied to the removal of Norfloxacin in chloride media by electro-oxidation. Chemosphere 249, 126178. https://doi.org/10.1016/j.chemosphere.2020.126178.

Catalan, G., Scott, J.F., 2009. Physics and applications of bismuth ferrite. Adv. Mater. 21, 2463–2485. https://doi.org/10.1002/adma.200802849.

Daghrir, R., Drogui, P., Robert, D., 2012. Photoelectrocatalytic technologies for environmental applications. J. Photochem. Photobiol. Chem. 238, 41–52. https://doi.org/10.1016/j.jphotochem.2012.04.009.

Deepak Sharma, A., Basantakumar Sharma, H., 2022. Influence of sintering temperature on structural, morphological and optical properties of nanocrystalline bismuth ferrite thin films via sol-gel processing. IOP Conf. Ser. Mater. Sci. Eng. 1219, 012052 https://doi.org/10.1088/1757-899x/1219/1/012052.

Farhadi, A.R.K., Rahemi, N., Allahyari, S., Tasbihi, M., 2021. Metal-doped perovskite $BiFeO_3$/rGO nanocomposites towards the degradation of acetaminophen in aqueous phase using plasma-photocatalytic hybrid technology. J. Taiwan Inst. Chem. Eng. 120, 77–92. https://doi.org/10.1016/j.jtice.2021.03.021.

Gong, J., Zhang, J., Lin, H., Yuan, J., 2018. "Cooking carbon in a solid salt": synthesis of porous heteroatom-doped carbon foams for enhanced organic pollutant degradation under visible light. Appl. Mater. Today 12, 168–176. https://doi.org/10.1016/j.apmt.2018.04.008.

Gulati, S., Goyal, K., Arora, A., Kumar, S., Trivedi, M., Jain, S., 2022. Bismuth ferrite ($BiFeO_3$) perovskite-based advanced nanomaterials with state-of-the-art photocatalytic performance in water cleanup. Environ. Sci. Water Res. Technol. https://doi.org/10.1039/d2ew00027j.

Gumiel, C., Calatayud, D.G., 2021. Thin film processing of multiferroic $BiFeO_3$: from sophistication to simplicity. A review. Bol. la Soc. Esp. Ceram. y Vidr. 1–25. https://doi.org/10.1016/j.bsecv.2021.08.002.

Guo, Y., Pu, Y., Cui, Y., Hui, C., Wan, J., Cui, C., 2017. A simple method using citric acid as the template agent to improve photocatalytic performance of $BiFeO_3$ nanoparticles. Mater. Lett. 196, 57–60. https://doi.org/10.1016/j.matlet.2017.03.023.

Harish, K.N., Bhojya Naik, H.S., Prashanth Kumar, P.N., Viswanath, R., 2012. Synthesis, enhanced optical and photocatalytic study of Cd-Zn ferrites under sunlight. Catal. Sci. Technol. 2, 1033–1039. https://doi.org/10.1039/c2cy00503d.

He, J., Guo, R., Fang, L., Dong, W., Zheng, F., Shen, M., 2013. Characterization and visible light photocatalytic mechanism of size-controlled $BiFeO_3$ nanoparticles. Mater. Res. Bull. 48, 3017–3024. https://doi.org/10.1016/j.materresbull.2013.04.058.

Huang, H., Scott, J.F., 2018. Ferroelectric Materials for Energy Applications. John Wiley & Sons.

Kim, Y., Yang, S., Kang, Y., Kim, B.K., Lee, H., 2018. Transition metal doped Sb@SnO_2 nanoparticles for photochemical and electrochemical oxidation of cysteine. Sci. Rep. 8, 1–8. https://doi.org/10.1038/s41598-018-30962-0.

Kumbhar, S.S., Mahadik, M.A., Shinde, S.S., Rajpure, K.Y., Bhosale, C.H., 2015. Fabrication of $ZnFe_2O_4$ films and its application in photoelectrocatalytic degradation of salicylic acid. J. Photochem. Photobiol., B 142, 118–123. https://doi.org/10.1016/j.jphotobiol.2014.12.002.

Lavaee, P., Danesh, N.M., Ramezani, M., Abnous, K., Taghdisi, S.M., 2017. Colorimetric aptamer based assay for the determination of fluoroquinolones by triggering the reduction-catalyzing activity of gold nanoparticles. Microchim. Acta 184, 2039–2045. https://doi.org/10.1007/s00604-017-2213-4.

Liao, X., Li, T.T., Ren, H.T., Mao, Z., Zhang, X., Lin, J.H., Lou, C.W., 2021. Enhanced photocatalytic performance through the ferroelectric synergistic effect of p-n heterojunction $BiFeO_3$/TiO_2 under visible-light irradiation. Ceram. Int. 47, 10786–10795. https://doi.org/10.1016/j.ceramint.2020.12.195.

Liu, H., Cheng, S., Wu, M., Wu, H., Zhang, J., Li, W., Cao, C., 2000. Photoelectrocatalytic degradation of sulfosalicylic acid and its electrochemical impedance spectroscopy investigation. J. Phys. Chem. A 104, 7016–7020. https://doi.org/10.1021/jp000171q.

Liu, T., Xu, Y., Feng, S., Zhao, J., 2011. A facile route to the synthesis of $BiFeO_3$ at low temperature. J. Am. Ceram. Soc. 94, 3060–3063. https://doi.org/10.1111/j.1551-2916.2011.04536.x.

Ma, D., Yi, H., Lai, C., Liu, X., Huo, X., An, Z., Li, L., Fu, Y., Li, B., Zhang, M., Qin, L., Liu, S., Yang, L., 2021. Critical review of advanced oxidation processes in organic wastewater treatment. Chemosphere 275, 130104. https://doi.org/10.1016/j.chemosphere.2021.130104.

Malviya, K.D., Klotz, D., Dotan, H., Shlenkevich, D., Tsyganok, A., Mor, H., Rothschild, A., 2017. Influence of Ti doping levels on the photoelectrochemical properties of thin-film hematite (α-Fe_2O_3) photoanodes. J. Phys. Chem. C 121, 4206–4213. https://doi.org/10.1021/acs.jpcc.7b00442.

Montañés, M.T., García-Gabaldón, M., Roca-Pérez, L., Giner-Sanz, J.J., Mora-Gómez, J., Pérez-Herranz, V., 2020. Analysis of norfloxacin ecotoxicity and the relation with its degradation by means of electrochemical oxidation using different anodes. Ecotoxicol. Environ. Saf. 188, 109923 https://doi.org/10.1016/j.ecoenv.2019.109923.

Mora-Gómez, J., Escribá-Jiménez, S., Carrillo-Abad, J., García-Gabaldón, M., Montañés, M.T., Mestre, S., Pérez-Herranz, V., 2022. Study of the chlorfenvinphos pesticide removal under different anodic materials and different reactor configuration. Chemosphere 290. https://doi.org/10.1016/j.chemosphere.2021.133294.

Mora-Gómez, J., García-Gabaldón, M., Carrillo-Abad, J., Montañés, M.T., Mestre, S., Pérez-Herranz, V., 2020. Influence of the reactor configuration and the supporting electrolyte concentration on the electrochemical oxidation of Atenolol using BDD and SnO_2 ceramic electrodes. Separ. Purif. Technol. 241 https://doi.org/10.1016/j.seppur.2020.116684.

Mora-Gomez, J., Ortega, E., Mestre, S., Pérez-Herranz, V., García-Gabaldón, M., 2019. Electrochemical degradation of norfloxacin using BDD and new Sb-doped SnO_2 ceramic anodes in an electrochemical reactor in the presence and absence of a cation-exchange membrane. Separ. Purif. Technol. 208, 68–75. https://doi.org/10.1016/j.seppur.2018.05.017.

Nkwachukwu, O.V., Muzenda, C., Ojo, B.O., Zwane, B.N., Koiki, B.A., Orimolade, B.O., Nkosi, D., Mabuba, N., Arotiba, O.A., 2021. Photoelectrochemical Degradation of Organic Pollutants on a La3+ Doped BiFeO3 Perovskite. Catalysts 2021, 11, 1069. doi:10.3390/ catal11091069.

Pradhan, A.K., Zhang, K., Hunter, D., Dadson, J.B., Loiutts, G.B., Bhattacharya, P., Katiyar, R., Zhang, J., Sellmyer, D.J., Roy, U.N., Cui, Y., Burger, A., 2005. Magnetic and electrical properties of single-phase multiferroic $BiFeO_3$. J. Appl. Phys. 97 https://doi.org/10.1063/1.1881775.

Sharmin, F., Basith, M.A., 2022. Highly efficient photocatalytic degradation of hazardous industrial and pharmaceutical pollutants using gadolinium doped $BiFeO_3$ nanoparticles. J. Alloys Compd. 901, 163604 https://doi.org/10.1016/j.jallcom.2021.163604.

Shurbaji, S., Huong, P.T., Altahtamouni, T.M., 2021. Review on the visible light photocatalysis for the decomposition of ciprofloxacin, norfloxacin, tetracyclines, and sulfonamides antibiotics in wastewater. Catalysts 11, 437. https://doi.org/10.3390/catal11040437.

Soltani, T., Lee, B.K., 2020. Ag-doped $BiVO_4$/$BiFeO_3$ photoanode for highly efficient and stable photocatalytic and photoelectrochemical water splitting. Sci. Total Environ. 736 https://doi.org/10.1016/j.scitotenv.2020.138640.

Su, Y. fan, Wang, Kuo, G.B., Chang, D.T.F., Shih, M. ling, hsin, Y., 2016. Photoelectrocatalytic degradation of the antibiotic sulfamethoxazole using TiO_2/Ti photoanode. Appl. Catal. B Environ. 186, 184–192. https://doi.org/10.1016/j.apcatb.2016.01.003.

Tian, D., Zhou, H., Zhang, H., Zhou, P., You, J., Yao, G., Pan, Z., Liu, Y., Lai, B., 2022. Heterogeneous photocatalyst-driven persulfate activation process under visible light irradiation: from basic catalyst design principles to novel enhancement strategies. Chem. Eng. J. 428, 131166 https://doi.org/10.1016/j.cej.2021.131166.

Wang, D., Shen, H., Guo, L., Fu, F., Liang, Y., 2016. Design and construction of the sandwich-like Z-scheme multicomponent CdS/Ag/Bi_2MoO_6 heterostructure with enhanced photocatalytic performance in RhB photodegradation. New J. Chem. 40, 8614–8624. https://doi.org/10.1039/c6nj01893a.

Wang, J.L., Xu, L.J., 2012. Advanced oxidation processes for wastewater treatment: formation of hydroxyl radical and application. Crit. Rev. Environ. Sci. Technol. 42, 251–325. https://doi.org/10.1080/10643389.2010.507698.

Wang, Y., Zhang, M., Yue, Y., Zhang, H., Mahajan, A., Dunn, S., Yan, H., 2022. Chemical solution deposition of single phase $BiFeO_3$ thin films on transparent substrates. Sol. RRL. https://doi.org/10.1002/solr.202200124.

Wu, J., Wang, J., Xiao, D., Zhu, J., 2012. A method to improve electrical properties of $BiFeO_3$ thin films. ACS Appl. Mater. Interfaces 4, 1182–1185. https://doi.org/10.1021/am300236j.

Xu, J., Sun, M., Zhang, C., Wu, M., Fu, D., 2022. Electrochemical mineralization of direct blue 71 with boron-doped diamond anodes: factor analysis and mechanisms study. J. Environ. Chem. Eng. 10, 107031 https://doi.org/10.1016/j.jece.2021.107031.

Yu, Han, Dou, D., Zhang, X., Zhang, L., Dong, H., Yu, Hongbing, 2020. Degradation of Norfloxacin in saline water by synergistic effect of anode and cathode in a novel photo-electrochemical system. J. Clean. Prod. 242, 118548 https://doi.org/10.1016/j.jclepro.2019.118548.

Zeng, T., Yu, X., Ye, K.-H., Qiu, Z., Zhu, Y., Zhang, Y., 2015. $BiPO_4$ film on ITO substrates for photoelectrocatalytic degradation. Inorg. Chem. Commun. 58, 39–42. https://doi.org/10.1016/j.inoche.2015.04.027.

Zhang, Q., Zhou, M., Du, X., Su, P., Fu, W., Song, G., 2022. Highly efficient dual-cathode Electro-Fenton process without aeration at a wide pH range: simultaneously enhancing Fe(II) regeneration and mineralization efficiency. Chem. Eng. J. 429, 132436 https://doi.org/10.1016/j.cej.2021.132436.

Zhang, Y., Yi, Z., Wu, G., Shen, Q., 2016. Novel Y doped $BiVO_4$ thin film electrodes for enhanced photoelectric and photocatalytic performance. J. Photochem. Photobiol. Chem. 327, 25–32. https://doi.org/10.1016/j.jphotochem.2016.05.004.

Zhao, X., Qu, J., Liu, H., Hu, C., 2007a. Photoelectrocatalytic degradation of triazine-containing azo dyes at gamma-Bi_2MoO_6 film electrode under visible light irradiation (lamda > 420 nm). Environ. Sci. Technol. 41, 6802–6807. https://doi.org/10.1021/es070598b.

Zhao, X., Xu, T., Yao, W., Zhang, C., Zhu, Y., 2007b. Photoelectrocatalytic degradation of 4-chlorophenol at Bi_2WO_6 nanoflake film electrode under visible light irradiation. Appl. Catal. B Environ. 72, 92–97. https://doi.org/10.1016/j.apcatb.2006.10.006.

Zhao, X., Zhu, Y., 2006. Synergetic degradation of rhodamine B at a porous $ZnWO_4$ film electrode by combined electro-oxidation and photocatalysis. Environ. Sci. Technol. 40, 3367–3372. https://doi.org/10.1021/es052029e.

Zhu, F., Lv, Y., Li, J., Ding, J., Xia, X., Wei, L., Jiang, J., Zhang, G., Zhao, Q., 2020. Enhanced visible light photocatalytic performance with metal-doped Bi_2WO_6 for typical fluoroquinolones degradation: efficiencies, pathways and mechanisms. Chemosphere 252, 126577. https://doi.org/10.1016/j.chemosphere.2020.126577.